International Journal of Microwave and Wireless Technologies

cambridge.org/mrf

Planar 180° hybrid coupler with non-interspersed ports for millimeter-wave applications

Jaber Moghaddasi and Ke Wu

PolyGrames Research Centre, Department of Electrical Engineering, Polytechnique Montreal, University of Montreal, 2500 Ch. De Polytechnique, Montreal, QC, Canada

Research Paper

Cite this article: Moghaddasi J, Wu K (2020). Planar 180° hybrid coupler with non-interspersed ports for millimeter-wave applications. *International Journal of Microwave and Wireless Technologies* **12**, 293–302. https://doi.org/10.1017/S1759078719001533

Received: 23 April 2019
Revised: 8 November 2019
Accepted: 16 November 2019
First published online: 11 December 2019

Key words:
Passive components and circuits

Author for correspondence:
Jaber Moghaddasi,
E-mail: jaber.moghaddasi@polymtl.ca

Abstract

This paper presents a simple topology of 180° hybrid coupler with non-interspersed inputs and outputs, as opposed to the conventional rat-race topology. Such hybrid coupler topologies with inputs located on one side and outputs at the opposite side simplify the design of signal routings and module packaging when integrated with other circuits and components. It also relaxes the necessity of using auxiliary compensating components such as tapers, jumpers, and crossovers. The proposed coupler topology is theoretically analyzed through a *T*-matrix approach. The analysis comes up with design equations and diagrams that help choose the structural parameters for the desired specification. The simplicity and also the immunity against intrinsic parasitic effects within the proposed topology make it an excellent candidate for operation over any RF and millimeter-wave frequency bands, for applications such as automotive radar or *E*-band backhaul radio. To this end, a coupler based on the proposed scheme is realized for operation over 77 GHz and assessed through on-wafer measurements. Good agreement of the measured results with the simulated and analytical counterparts demonstrates the superior performance of the proposed 180° hybrid coupler.

Introduction

The four-port rat-race (or ring hybrid which is a form of 180° coupler) and 180° hybrid couplers provide the sum and difference in operations of two input signals at two isolated ports. In other words, they create 180° relative phase difference between the signals at the output ports for a signal arriving at one input port and 0° relative phase difference for a signal arriving at the other input port. This relative phase difference between the output signals is 90° for the 90° quadrature hybrid coupler. But, with the 180° hybrid coupler, if two distinct signals are incident at two input ports, two equally divided portions of each input signal appear at the two output ports. One pair of output signals, each including two portions from the two input signals, is out of phase while the two other output signals are in phase. The principle and the *S*-matrix of the conventional 180° hybrid coupler (rat-race) are described in [1]. This hybrid coupler with its specific phasing network between all ports has found application in many types of RF and microwave signal routing-based integrated circuits such as balanced mixers [2], multiport interferometers [3], and in-phase/quadrature mixers [4].

The 180° hybrid couplers have been investigated for different aspects including bandwidth enhancement using coupled lines [5], broadband phase inverter [6–11], size reduction using shunt open stubs [12, 13], spurious suppression [14], and arbitrary power division [15, 16].

One of the main drawbacks of the conventional topology of the ring-shaped rat-race coupler is related to the respective position of input–output ports, which makes laying out complicated when applied to the interconnects, integration, and packaging of microwave circuits. This demands for multilayer circuits or utilization of crossovers and/or vias, which may unfortunately bring up other limitations especially in high-frequency circuits. Therefore, this aspect has recently come into light and novel topologies of 180° hybrid couplers with non-interspersed ports have been developed, which are configured through cascading couplers and phase shifters, in essence.

Such different topologies of 180° hybrid coupler were first introduced by [17] in which non-interspersed ports were obtained by two-section hybrids using cascaded hybrid rings. Another configuration of a pair of cascaded microstrip coupled line couplers and one 180° phase shifter was reported by [18]. This topology that still suffers from the location of input–output ports is shown in Fig. 1(a) for reference. Based on this topology, multilayer hybrid couplers were developed and implemented using the multilayer low-temperature co-fired ceramic (LTCC) technology [4]. Within multilayer implementation of the topology in Fig. 1(a), a pair of input and output was implemented in one layer and the other pair in

© Cambridge University Press and the European Microwave Association 2019

CAMBRIDGE UNIVERSITY PRESS

the other layer. To position the pair of inputs in one layer and the pair of outputs in another layer, the interconnections between three sections were rewired in an improved topology as it is shown in Fig. 1(b). However, such topology has limited applications and may not be used within single-layer circuits.

A near-TEM Lange hybrid was also reported in [19]. However, the use of vias for interlayer connection or bond-wires limits the frequency of operation and increases the gain and phase imbalances due to the parasitic inductance in vias. Another topology comprising of a weak-coupling parallel coupled line and a strong-coupling trans-directional (TRD) coupler connected with a 180° phase shifter was proposed by [20]. This topology is depicted in Fig. 1(c). The use of periodic shunt capacitor components in TRD relaxes the necessity of tightly coupled lines and allows for the use of a single-layer printed circuit board (PCB) technique without any vias or bond wires. However, the capacitors may fail to operate at very high frequencies and increase the cost.

In this paper, an alternative topology of rat-race with non-interspersed ports is proposed, which is sketched in Fig. 1(d). The proposed topology can be categorized in the same family of newly introduced hybrid couplers that are essentially built up through cascading couplers and phase shifters. The proposed hybrid topology does not require any vias, bond-wires, or lumped components and facilitates implementation on a single layer of substrate for interconnection, integration, and packaging purposes, especially for high-frequency circuits.

The principles of this topology are discussed along with analytical solutions in the next sections. The proposed coupler is also implemented in this work using our in-house technology of Miniaturized Hybrid Microwave Integrated Circuit (MHMIC) to demonstrate its performances around 77 GHz. Measurement results of the prototyped 180° hybrid coupler are presented.

Principles of the proposed topology of 180° hybrid coupler

As it is shown in Fig. 1(d), the proposed topology of 180° hybrid coupler is comprised of one quadrature coupler and two 90° phase shifters. With this configuration, two input ports can be located on one side and outputs on the other side. As opposed to the previously reported structures, which were mainly based on backward-coupled line couplers, the quadrature coupler in the proposed topology is a forward coupler. This configuration can be implemented with both TEM- or quasi-TEM mode structures, such as microstrip, and non-TEM structures, such as substrate-integrated waveguide. In this work, TEM-mode-based structures are selected to realize the proposed 180° coupler topology at millimeter-wave frequencies. Figure 2 shows the TEM-mode-based topology of the 180° hybrid coupler, which consists of wideband Schiffman phase shifters [21–28] and a quadrature branch-line coupler [1].

Theoretical analysis

To theoretically analyze the proposed 180° hybrid coupler, transfer T-matrix is derived that relates the output port power wave variables to the input port power wave variables of a network [29]. It should be highlighted that the standard definition of T-matrix of the four-port network is defined in accordance with [30, eq. 8] herein, and the ports reference impedances in our analysis are identical. In view of the above, the structure shown in Fig. 2 is first divided into three distinct segments, then the overall T-matrix is derived from the multiplication of three matrices, i.e. $T1 \times T2 \times T3$. The T-matrix of each can be derived as it is briefly explained next.

T-matrix of the first segment (T1)

First segment consists of a Schiffman phase shifter and a transmission line with an electrical length of θ_3. T-matrix of the Schiffman phase shifter can be obtained by converting the ABCD parameters of coupled-line with connected end-ports that were reported by [31] into T-parameters using the equations from [32, 33].

The matrix $T1$ can be expressed as in (1) where Z_e and Z_o denote the even and odd mode impedances of the coupled-line in the phase shifter part and Z_0 is the characteristic impedance of the transmission line.

$$T1 = \begin{bmatrix} T1sh_{11} & 0 & 0 & 0 \\ 0 & T1sh_{22} & 0 & T1sh_{24} \\ 0 & 0 & T1sh_{33} & 0 \\ 0 & T1sh_{42} & 0 & T1sh_{44} \end{bmatrix} \quad (1)$$

$$\begin{aligned}
T1sh_{11} &= (\cos(\theta_3) - j\sin(\theta_3))(\cos(\theta_2) - j\sin(\theta_2)) \\
T1sh_{22} &= \frac{(\cos(\theta_3) - jsin(\theta_3))(Z_0 Z_e \cot(\theta_c) - j(Z_0^2 + Z_e Z_o - jZ_0 Z_o tan(\theta_c)))}{Z_0(Z_e cot(\theta_1) + Z_o tan(\theta_c))} \\
T1sh_{24} &= \frac{(Z_0^2 - Z_e Z_o)(-j\cos(\theta_3) + \sin(\theta_3))}{Z_0(Z_e cot(\theta_1) + Z_o tan(\theta_1))} \\
T1sh_{33} &= (\cos(\theta_3) + j\sin(\theta_3))(\cos(\theta_2) + j\sin(\theta_2)) \\
T1sh_{42} &= \frac{(Z_0^2 - Z_e Z_o)(j\cos(\theta_3) + \sin(\theta_3))}{Z_0(Z_e cot(\theta_c) + Z_o tan(\theta_1))} \\
T1sh_{44} &= \frac{(\cos(\theta_3) + jsin(\theta_3))(Z_0 Z_e \cot(\theta_1) + j(Z_0^2 + Z_e Z_o + jZ_0 Z_o tan(\theta_1)))}{Z_0(Z_e cot(\theta_1) + Z_o tan(\theta_1))}.
\end{aligned}$$

https://doi.org/10.1017/S1759078719001533 Published online by Cambridge University Press

T-matrix of second segment (T2)

The matrix $T2$ can be obtained through multiplying the submatrices of $T21 \times T22 \times T21$. $T22$ pertains to the T-matrix of a pair of transmission lines with a characteristic impedance of $Z0/\sqrt{2}$ and identical electrical lengths θ while $T21$ denotes the T-matrix of one branch of a branch line directional coupler with characteristic impedance of Z_0 and electrical length θ that can be found in [29]. Hence, the matrix $T2$ can be expressed by

$$T2 = \begin{bmatrix} Th_{11} & Th_{12} & Th_{13} & Th_{14} \\ Th_{12} & Th_{11} & Th_{14} & Th_{13} \\ -Th_{13} & -Th_{14} & Th_{33} & Th_{34} \\ -Th_{14} & -Th_{13} & Th_{34} & Th_{33} \end{bmatrix} \tag{2}$$

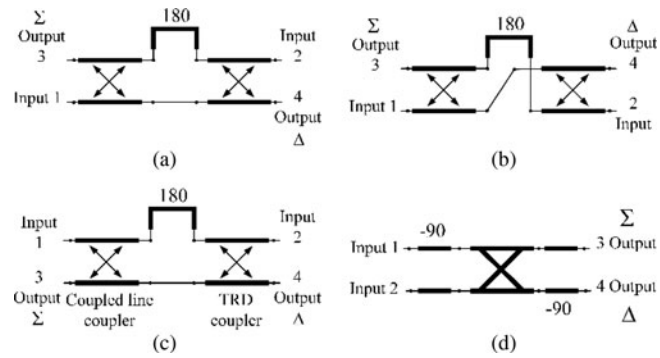

Fig. 1. The 180° hybrid couplers with typical topologies and input/output ports. (a) [18], (b) [4], (c) [20], (d) This paper.

$$Th_{11} = \cos(\theta)(1 - j\cot(-\theta)) + \frac{\sin(\theta)(\sin^2(-\theta)(0.5j\cot^2(-\theta) - \cot(-\theta) - 1.5j) + 0.5j)}{\sqrt{2}\sin^2(-\theta)}$$

$$Th_{12} = \frac{\sin(\theta)(1 - j\cot(-\theta)) + j\cos(\theta)\sqrt{2}}{\sqrt{2}\sin(-\theta)}$$

$$Th_{13} = -j\cot(-\theta)\cos(\theta) + \frac{\sin(\theta)(\sin^2(-\theta)(0.5j\cot^2(-\theta) - 0.5j) + 0.5j)}{\sqrt{2}\sin^2(-\theta)}$$

$$Th_{14} = \frac{-j\cot(-\theta)\sin(\theta) + j\cos(\theta)\sqrt{2}}{\sqrt{2}\sin(-\theta)}$$

$$Th_{33} = \cos(\theta)(1 + j\cot(-\theta)) + \frac{\sin(\theta)(\sin^2(-\theta)(-0.5j\cot^2(-\theta) - \cot(-\theta) + 1.5j) - 0.5j)}{\sqrt{2}\sin^2(-\theta)}$$

$$Th_{34} = \frac{\sin(\theta)(1 + j\cot(-\theta)) - j\cos(\theta)\sqrt{2}}{\sqrt{2}\sin(-\theta)}.$$

T-matrix of third segment (T3)

The matrix $T3$ pertains to another phase shifter which is connected at the output port of the branch-line hybrid coupler via a transmission line with a length of θ_3. The matrix $T3$ can be

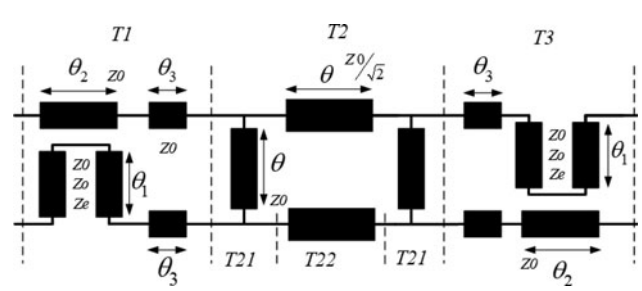

Fig. 2. Implementation of the proposed topology in TEM-mode structures.

https://doi.org/10.1017/S1759078719001533 Published online by Cambridge University Press

expressed as:

$$T3 = \begin{bmatrix} T3sh_{11} & 0 & T3sh_{13} & 0 \\ 0 & T3sh_{22} & 0 & 0 \\ T3sh_{31} & 0 & T3sh_{33} & 0 \\ 0 & 0 & 0 & T3sh_{44} \end{bmatrix} \quad (3)$$

$$T3sh_{11} = \frac{(\cos(\theta_3) - jsin(\theta_3))(Z_0 Z_e \cot(\theta_1) - j(Z_0^2 + Z_e Z_o - jZ_0 Z_o tan(\theta_1)))}{Z_0(Z_e cot(\theta_1) + Z_o tan(\theta_1))}$$

$$T3sh_{22} = (\cos(\theta_3) - j\sin(\theta_3))(\cos(\theta_2) - j\sin(\theta_2))$$

$$T3sh_{13} = -\frac{j(Z_0^2 - Z_e Z_o)(\cos(\theta_3) - jsin(\theta_3))}{Z_0(Z_e cot(\theta_1) + Z_o tan(\theta_1))}$$

$$T3sh_{31} = \frac{j(Z_0^2 - Z_e Z_o)(\cos(\theta_3) + jsin(\theta_3))}{Z_0(Z_e cot(\theta_1) + Z_o tan(\theta_1))}$$

$$T3sh_{33} = \frac{(\cos(\theta_3) + jsin(\theta_3))(Z_0 Z_e \cot(\theta_1) + j(Z_0^2 + Z_e Z_o + jZ_0 Z_o tan(\theta_1)))}{Z_0(Z_e cot(\theta_1) + Z_o tan(\theta_1))}$$

$$T3sh_{44} = (\cos(\theta_3) + j\sin(\theta_3))(\cos(\theta_2) + j\sin(\theta_2)).$$

All derived analytical T parameters are verified through comparison with the simulated ones in ADS for validation purposes.

Finally, the overall T-matrix of the proposed 180° hybrid coupler can be formulated by multiplying three matrices via arithmetic tools such as Mathematica. Due to the complexity of the resulting equations, they are not brought in here. However, the derived T-matrix would be helpful for computer-aided design when the conditions of 90° phase shifters and branch-line couplers are applied.

The phase difference between signals at the output ports of the Schiffman phase shifter was formulated in [21], which reads as

$$\Delta\varphi = K\theta_1 - \cos^{-1}\left(\frac{R - \tan(\theta_1)^2}{R + \tan(\theta_1)^2}\right), \quad (4)$$

where $K = \theta_2/\theta_1$ and $R = Z_e/Z_o$. For 90° phase shifter, K and θ_1 are selected to be 3 and $\pi/2$ at the center frequency, respectively. At the center frequency, where θ and θ_1 are $\pi/2$ and θ_2 is $3\pi/2$, the T-matrix of the proposed 180° hybrid coupler would be

$$T = \frac{1}{\sqrt{2}} \begin{bmatrix} -e^{-2j\theta_3} & e^{-2j\theta_3} & 0 & 0 \\ -e^{-2j\theta_3} & -e^{-2j\theta_3} & 0 & 0 \\ 0 & 0 & -e^{2j\theta_3} & e^{2j\theta_3} \\ 0 & 0 & -e^{2j\theta_3} & -e^{2j\theta_3} \end{bmatrix} \quad (5)$$

Substituting the T-matrix elements into the T-to-S parameter conversion equations in [30], one can yield

$$[S] = \frac{-e^{-2j\theta_3}}{\sqrt{2}} \begin{bmatrix} 0 & 0 & 1 & -1 \\ 0 & 0 & 1 & 1 \\ 1 & 1 & 0 & 0 \\ -1 & 1 & 0 & 0 \end{bmatrix}, \quad (6)$$

which confirms the hybrid is matched at input ports 1 and 2. Moreover, (6) shows that at output port 4, there is a 180° phase difference between the input signals from ports 1 and 2, whereas this phase difference is zero at output port 3. The S-matrix in (6) is almost the same as that of the classic ring hybrid. The only difference is that the signals at the output ports are either in-phase or out-of-phase with respect to the input signals, whereas the output signals in the classic ring hybrid are in quadrature phase with the input signal [1].

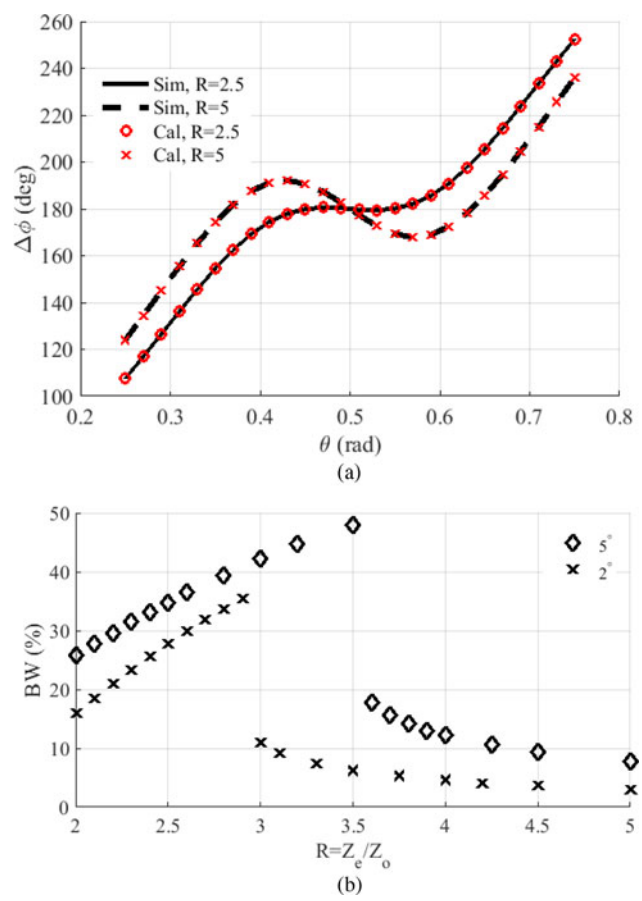

Fig. 3. Changes in phase difference and bandwidth for two different values of R. (a) Phase difference control and comparison between results of simulation and analytical equations. (b) Bandwidth control over R for (δ) of ±2° and ±5°, obtained from analytical analysis in (7).

https://doi.org/10.1017/S1759078719001533 Published online by Cambridge University Press

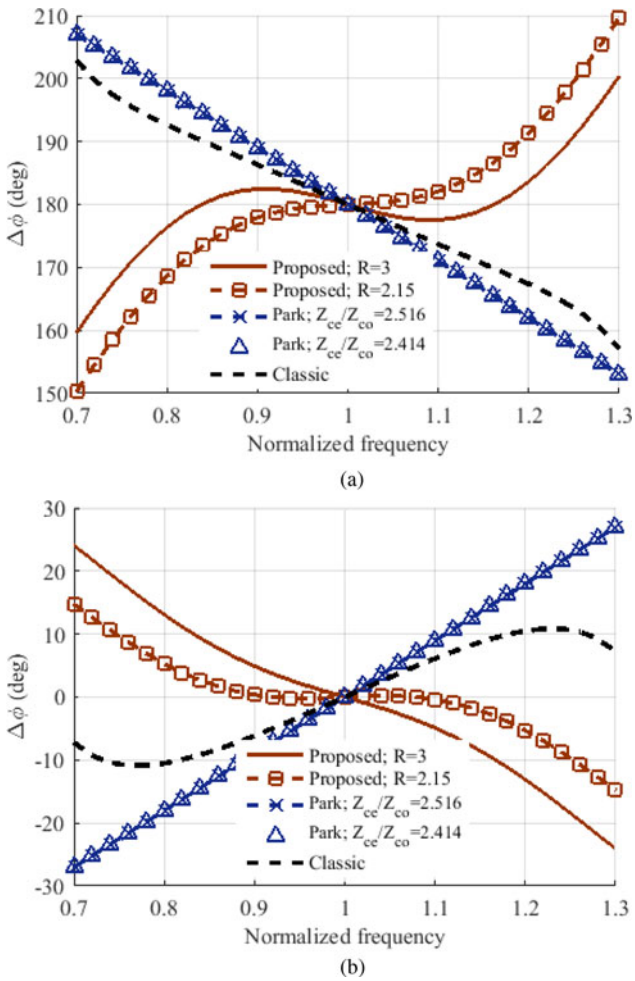

Fig. 4. Comparison of phase difference between our proposed 180° hybrid topology with the one proposed by Park in [18] and the classic rat-race. (a) Out-of-phase, (b) in-phase.

To examine the phase difference characteristic of the proposed 180° hybrid at frequencies other than the center frequency, the derived overall T-matrix of the proposed hybrid is converted to S-matrix through conversion equations from [30] via arithmetic tools such as Mathematica. It should be noted that at frequencies other than the center frequency, the condition of $\theta_1 = \theta$ and $\theta_2 = 3\theta$ remains valid. In addition, the coupled line is matched when $Z_0 = \sqrt{Z_o Z_e}$ [21]. Under these conditions, the phase difference at output ports 3 and 4 can be formulated from the S-matrix of the proposed hybrid as in the following:

$$\Delta = \angle S_{13} - \angle S_{14}$$

$$\angle S_{13} = \angle\left[\frac{(-0.54582 + j1.31773\cot(\theta))\csc(\theta)^2}{(\Phi_1 + \Phi_2 + \Phi_3)(\cos(3\theta) + j\sin(3\theta))^2}\right]$$

$$\Phi_1 = 0.614047 + j2.52241\cot(\theta)^3 + \cot(\theta)^4 - 0.136455\csc(\theta)^2$$

$$\Phi_2 = 0.0682275\csc(\theta)^4 + \cot(\theta)^2(-3.15786 - 1.06823\csc(\theta)^2)$$

$$\Phi_3 = \cot(\theta)(-j1.97659 - j0.658863\csc(\theta)^2), \tag{7-a}$$

$$\angle S_{14} = \angle\left[\frac{jZ0(1 + R\cot(\theta)^2)csc(\theta)(\Psi_1)}{(\Psi_2)(\Psi_3 + \Psi_4 + \Psi_5)(\cos(3\theta) + j\sin(3\theta))}\right]$$

$$\Psi_1 = -0.783612 + j1.2612\cot(\theta) + \cot(\theta)^2 + 0.261204\csc(\theta)^2$$

$$\Psi_2 = -Z0 + j2Z_e\cot(\theta) + RZ0\cot(\theta)^2$$

$$\Psi_3 = 0.614047 + j2.52241\cot(\theta)^3 + \cot(\theta)^4 - 0.136455\csc(\theta)^2$$

$$\Psi_4 = 0.0682275\csc(\theta)^4 + \cot(\theta)^2(-3.15786 - 1.06823\csc(\theta)^2)$$

$$\Psi_5 = \cot(\theta)(-j1.97659 - j0.658863\csc(\theta)^2). \tag{7-b}$$

One can observe in (7) that the bandwidth of the 180° phase difference depends on the ratio of even to odd mode impedances, i.e. $R = Z_e/Z_o$. In Fig. 3(a), simulation results of the proposed hybrid with ideal components through the commercial package of ADS is compared with the analytical equations concluded in (7). The excellent agreement between simulation and analytical results for two different values of R validates the theoretical analysis throughout this paper.

The bandwidth in which the desired maximum deviation takes place can be determined by controlling R. Figure 3(b) shows the change of bandwidth versus different values of R, which is helpful in the design of the proposed coupler. It should be noted that

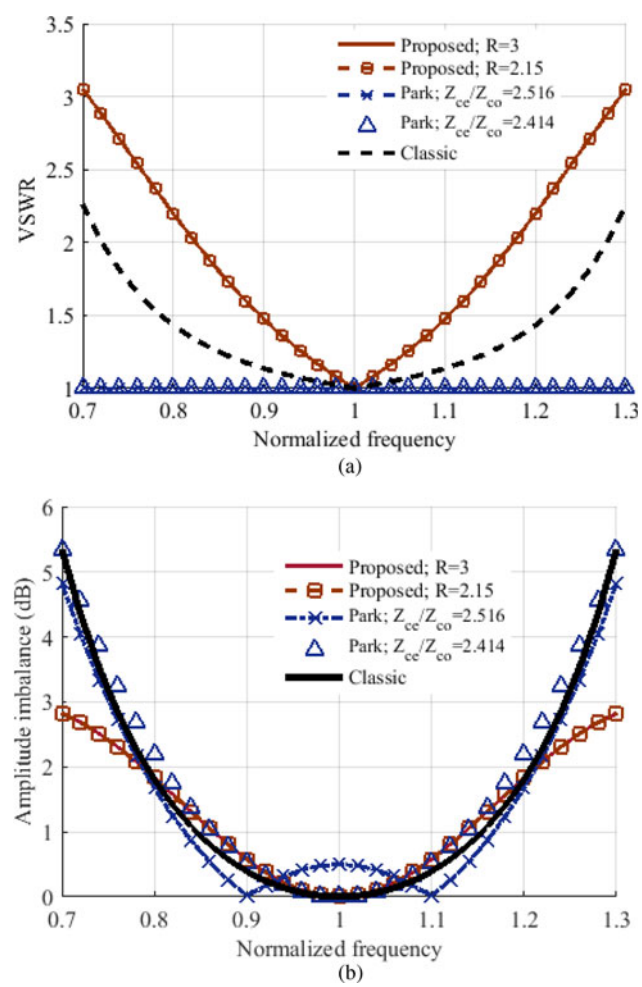

Fig. 5. Comparison between our proposed 180° hybrid topology with the one proposed by Park in [18] and the classic rat-race. (a) VSWR, (b) amplitude imbalance.

https://doi.org/10.1017/S1759078719001533 Published online by Cambridge University Press

Table 1. Comparison of the 180° hybrid couplers

Hybrid topology	Fractional BW (%)				
	VSWR < 1.22	VSWR < 1.5	Amplitude imbalance <0.5 dB	Phase deviation < ± 5° (180°)	Phase deviation < ± 5° (0°)
Rat-race	27.75	40	22.44	15.8	16.03
Coupled line [18] $\left(\frac{Zce}{Zco} = 2.414\right)^a$	100	100	19.57[b]	11.16	11.16
Coupled line [18] $\left(\frac{Zce}{Zco} = 2.516\right)^a$	100	100	27.56[c]	11.16	11.16
Proposed hybrid ($R = 2.15$)	10.4	20	18.56	28.77	39.19
Proposed hybrid ($R = 3$)	10.4	20	18.56	42.22	20.35

[a]Z_{ce} and Z_{co} are the even and odd mode impedances of the coupled-line couplers in the hybrid topology of [18], and $Z0^2 = Z_{ce} \times Z_{co}$.
[b]Under-coupled.
[c]Over-coupled.

abrupt changes in BW that can be observed in Fig. 3(b) are because the phase difference curves at maximum and minimum points exit the defined range of phase difference values, i.e. ±5° or ±2°.

Design of the proposed coupler

The proposed coupler has fairly a simple design procedure. To design the proposed coupler, the even and odd mode impedances of the coupled line should be determined per the desired bandwidth of the maximum tolerable deviation from the 180° phase difference. Figure 3 can be used to find a suitable ratio of even to odd mode impedances to achieve the desired bandwidth. On the other hand, a matching condition to the reference impedance (i.e. $Z_0 = \sqrt{Z_o Z_e}$) provides the second equation to determine the even and odd mode impedances and accordingly the coupling factor (C) of the coupled line (i.e. $C = -20\log[(R-1)/(R+1)]$). The electrical lengths of $\theta_1$and θ are 90° and θ_2 is 270°.

To discuss the characteristics of the proposed hybrid coupler, they are compared with other counterparts including classic rat-race and coupled-line from [18], based on simulations which are carried out using ideal blocks in ADS. Two different values of the ratio of even-to-odd mode impedances for each of the proposed hybrid (R) and the coupled-line hybrid (Zce/Zco)from [18] are considered for simulations and results are plotted in Fig. 4.

It can be observed in Figs 4(a) and 4(b) that the phase differences between output signals in the hybrid proposed by [18] are not affected by changes in the ratio of (Zce/Zco). Moreover, the bandwidth in which the maximum phase deviation of 5° occurs for both in-phase and out-of-phase components is slightly less than that of the rat-race hybrid coupler. However, the proposed hybrid has considerably larger bandwidth for both phase difference components with the same amount of deviation of 5°. This bandwidth can be controlled by changing R.

In Fig. 5(a), the hybrid couplers are compared in terms of matching at the input ports. One can see that the proposed hybrid has narrower bandwidth of VSWR with the value <1.22 (i.e. return loss >20 dB), while the hybrid coupler in [18] is completely matched given the condition $Z0^2 = Zce \times Zco$ is satisfied for any non-zero coupling factor, regardless of the length of the coupled lines. It should be pointed out the latter consequences can be concluded given the coupled line hybrid circuit of [18] is lossless.

Figure 5(b) demonstrates the performance of the hybrids in terms of amplitude imbalance for the output signals. The proposed hybrid coupler has less bandwidth of 0.5 dB amplitude imbalance when compared to the classic rat-race hybrid. This remains unaffected by changes in R, whereas the amplitude imbalance of the output signals in the hybrid coupler of [18] can be controlled by changing the ratio (Zce/Zco). This ratio in hybrid coupler of [18] can be set for a larger bandwidth of 0.5 dB amplitude imbalance than that of the classic rat-race hybrid.

These characteristics of studied hybrids are summarized in Table 1 in terms of fractional bandwidth for comparison purposes. One can observe that the examined hybrids may not satisfy all desired specifications with an identical percentage of bandwidth. For instance, the structure in [18] has acceptable phase differences in limited bandwidth of only around 11% even though excellent matching is readily achievable across the whole band. Our proposed hybrid can have wider bandwidth for phase differences, but in a narrower bandwidth, it satisfies the desired input matching specification. Obviously, the bandwidth in which all specifications are satisfied is dominated by the narrowest bandwidth, e.g. 11.16% for coupler in [18]. Interestingly enough, our proposed coupler shows to be capable of satisfying all specifications in a wider bandwidth, i.e. 20%, than other couplers if the input VSWR of 1.5:1 is considered to be sufficient.

It is also worth noticing that the only characteristic that is affected by the value of R is the phase difference at the output ports, whereas VSWR and gain balance remain unchanged with the changes in R. Furthermore, the changes in the bandwidth of phase differences are in the opposite direction. In other words, increasing R to larger values than 2.15 would increase the 180° phase difference, but reduces the bandwidth of 0° phase difference. Therefore, selecting the optimum value of R depends on the desired phase differences. Nevertheless, designer can conclude the approximate starting design value of R that can satisfy the desired bandwidth for either phase differences, using the information herein.

Prototyping and measurements

As it has already been mentioned, the proposed topology can outperform other existing counterparts as the design frequency increases, because no via, wire-bonding, or lumped elements are essentially used that can affect matching, phase, and amplitude imbalance. Therefore, the proposed hybrid was designed and implemented for operation around 77 GHz, using our in-house MHMIC fabrication process on an Alumina ceramic substrate

https://doi.org/10.1017/S1759078719001533 Published online by Cambridge University Press

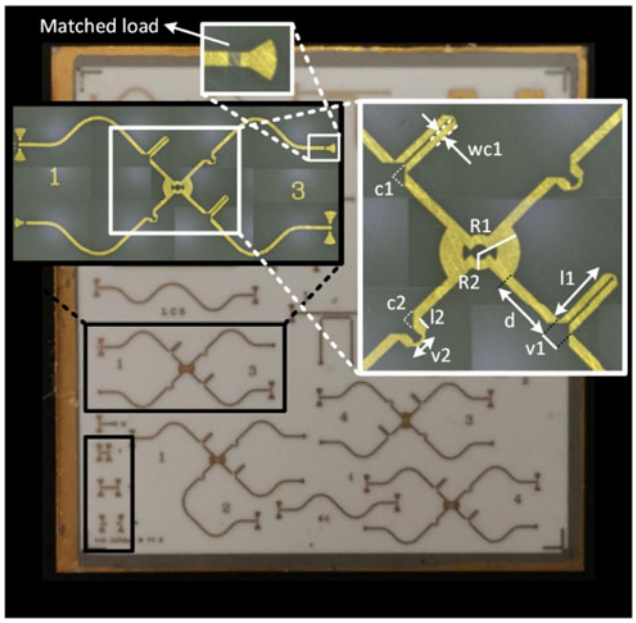

Fig. 6. Prototyped hybrid on ceramic die; ports #1, #2, #3, #4 in layout correspond to ports #1, #3, #4, #2, respectively, in standard port definition from [30]. $R1 = 393.7$ µm, $R2 = 172.7$ µm, $d = 624.8$ µm, $v1 = 162.6$ µm, $l1 = 1.46$ mm, $l2 = 94$ µm, $v2 = 647.7$ µm, $C1 = 142.24$ µm, $C2 = 114.3$ µm, $wc1 = 68.6$ µm.

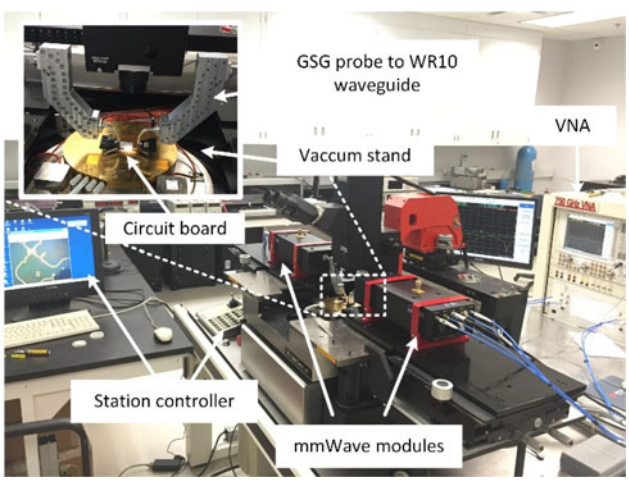

Fig. 7. Measurement setup which is held on mm-wave probing station.

with a permittivity of around 9.9 and a thickness of 0.254 mm. Through our in-lab MHMIC process, circuits with minimum microstrip linewidth of 20 µm can be prototyped. The prototyped MHMIC die is displayed in Fig. 6. Small modifications in the original configuration at the input of phase shifter are made within the optimization process in simulations.

To measure the *S*-parameters through two-port VNA, a few circuits are fabricated on the same die. The microscopic view shows one of the circuits with details. The measuring ports are connected to the designed coplanar adaptor while the unused ports are loaded with integrated matched resistors and RF grounds. The quadrature round-shaped coupler with a branch-line impedance of 70.7 Ω was designed for this frequency of operation. To minimize the radiation loss of the microstrip

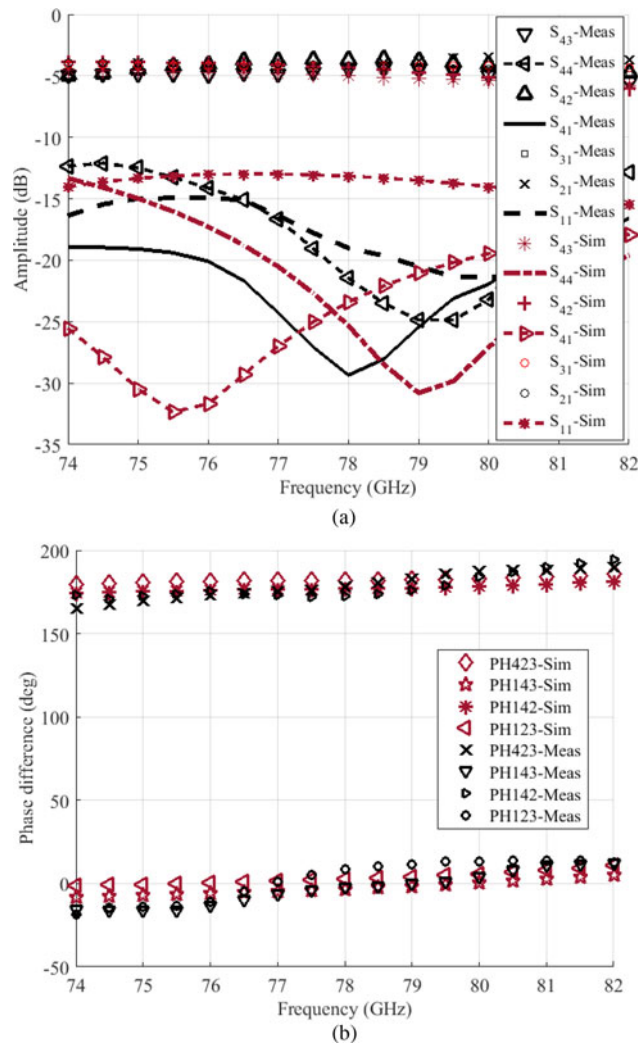

Fig. 8. Comparison of measured and simulated of *S*-parameters. (a) Amplitude, (b) phase differences: $PH423 = S_{42} - S_{43}$, $PH123 = S_{12} - S_{13}$, $PH142 = S_{12} - S_{42}$, $PH143 = S_{13} - S_{43}$.

transmission line, the reference characteristic impedance was selected to be 70.7 Ω.

To assess the performance of the prototyped hybrid, two-port on-wafer *S*-parameter measurement was carried out using the probe station (Karl Suss) with VNA (Agilent Technologies PNA-X, N5247A) shown in Fig. 7. To preserve the repeatability of amplitude and phase measurements, the Ground-Signal-Ground (GSG) probe (Picoprobe by GGB Industries-Model 120) with a pitch size of 150 µm was positioned on the same place over the coplanar adaptors with the same amount of pressure using high accuracy controllers. To de-embed the effect of transitions from the probe to the input ports of the designed hybrid, a standard Through-Reflect-Line (TRL) calibration kit was also designed on the same die for calibration purposes.

The phase and amplitude measurement results, corresponding to the port definition in Fig. 6, are shown in Figs 8(a) and 8(b). It should be noted that, ports #1, #2, #3, #4 in layout correspond to ports #1, #3, #4, #2, respectively within the standard port definition in [30].

The designed 180° hybrid is very well matched (return loss >10 dB) over 10 GHz bandwidth. At the center frequency of

https://doi.org/10.1017/S1759078719001533 Published online by Cambridge University Press

Table 2. Comparison of measured performances of 180° hybrid couplers

Hybrids	Design frequency (GHz)	Implementation technology	Fractional bandwidth (%)				Dimensions (guided wavelength λ_g)
			Return loss >15 dB	Isolation >20 dB	Phase imbalance 0 ± 5°	Phase difference 180 ± 5°	
[17]	2	Single-layer PCB with crossover	22.9	37.5	8.3		–
[18]	1	Single-layer PCB	25	40	9.9	11.7	–
[4]	24	LTCC	14 dB[a]	14.6 dB[a]	177°[a]		0.67 × 0.54
[19]	8	LTCC	20[b]	35[b]	12.0[b]		0.69 × 0.59
[20]	2.4	Single-layer PCB	26.3	12.7	45.8	12.9	0.64 × 0.53
This work	77	MHMIC	10.25	6.41	4.5	5.19	1.86 × 1.86

[a]Only central frequency.
[b]Simulation results of the circuit in [19, Fig. 11].

78 GHz, the measured values of isolation are about 30 dB and the port-to-port insertion loss varies between 0.6 and 1.25 dB for all measured pairs of ports. Gain imbalance at the same frequency was measured to be 0.3 dB and it varies within the range of −0.4 to 1.25 dB throughout the whole 10 GHz bandwidth. The measured phase difference shown in Fig. 8 agrees well with the simulation values.

The performance of the prototyped device is compared with the recently reported 180° hybrids in Table 2 based on the measurement results, although the operational frequency of them is quite different. One can observe that with the tight condition of 5° deviation from phase differences of the output signals, it covers a fractional bandwidth of around 5% which corresponds to roughly 4 GHz bandwidth around 77 GHz. This is sufficient for applications such as automotive radar (i.e. 76–77 GHz) or backhaul radios (71–76 GHz). In these frequency bands, the prototyped hybrid can be matched with return loss values larger than 15 dB and isolation of better than 20 dB.

Table 2 shows that the prototype of the proposed hybrid possesses the least measured fractional bandwidth in terms of matching, isolation, or phase differences, in comparison to other works. Nevertheless, it has sufficient coverage over the application bandwidth.

It should be highlighted that none of the previously reported works was implemented in millimeter-wave frequency bands as this work did. The crossovers across the microstrip traces in [17], multilayer crossing in [4] and [19] to obtain non-interspersed ports or lumped capacitors in [20] can substantially degrade the performance of the device when designed within high-frequency regions. The coupler in [18] still suffers the problem of interspersed port positions as the conventional rat-race coupler does. The main drawback of the proposed topology is the extended size which can be improved using miniaturization techniques such as the one proposed by [34].

Conclusion

A topology of 180° hybrid coupler was introduced and analyzed throughout this work. The principles of the proposed hybrid were theoretically examined through the *S*-parameter analysis. The four-port *T*-matrix of the proposed hybrid was derived for conversion to *S*-matrix. The derived analytical equations help calculate the bandwidth in which the maximum tolerable deviation from 180° phase difference occurs. The theoretical analysis was validated when compared with simulation results with ideal components in commercial software. In addition, the characteristics of the proposed hybrid were compared with previously reported coupled-line 180° hybrids in terms of matching, phase, and gain imbalance when designed with ideal consisting blocks. The main application of such structure is in signal routing circuits operating at the millimeter-wave frequency band with respect to structure interconnection and integration, where already reported topologies of 180° hybrid couplers with non-interspersed input–output ports could fail due to their structural parasitic effects. Successful implementation of the prototyped hybrid on MHMIC die around 77 GHz makes the proposed topology a comparable candidate for applications in mixer, amplifiers, or multiport phasing networks in high-frequency integrated circuits

References

1. **Pozar DM** (1998) *Power Dividers and Directional Couplers, Microwave Engineering*, 2nd Edn. New York: Wiley Press, 362–375.
2. **Maas SA** (1993) *Microwave Mixers*, 2nd Edn. Norwood, MA: Artech House Press.
3. **Moghaddasi J and Wu K** (2013) Unified radar-communication (RadCom) multi-port interferometer transceiver. *Proc. Europ. Radar Conf.*, Nuremberg, Germany, Oct. 2013, 479–482.
4. **Napijalo V and Kearns B** (2008) Multilayer 180 hybrid coupler. *IEEE Transactions on Microwave Theory and Techniques* **56**, 2525–2535.
5. **March SA** (1968) Wideband stripline hybrid ring. *IEEE Transactions on Microwave Theory and Techniques* **MTT-16**, 361.
6. **Rehnmark S** (1977) Wide-band balanced line microwave hybrids. *IEEE Transactions on Microwave Theory and Techniques* **MTT-25**, 825–830.
7. **Ho C-H, Fan L and Chang K** (1994) New uniplanar coplanar waveguide hybrid-ring couplers and magic-T's. *IEEE Transactions on Microwave Theory and Techniques* **42**, 2440–2448.
8. **Heimer BR, Fan L and Chang K** (1997) Uniplanar hybrid couplers using asymmetrical coplanar striplines. *IEEE Transactions on Microwave Theory and Techniques* **45**, 2234–2240.
9. **Wang T and Wu K** (1999) Size-reduction and band-broadening design technique of uniplanar hybrid ring coupler using phase inverter for M(H)MIC's. *IEEE Transactions on Microwave Theory and Techniques* **47**, 198–206.

https://doi.org/10.1017/S1759078719001533 Published online by Cambridge University Press

10. **Chang C-Y and Yang C-C** (1999) A novel broad-band Chebyshev-response rat-race ring coupler. *IEEE Transactions on Microwave Theory and Techniques* **47**, 435–462.
11. **Mo TT, Xue Q and Chan CH** (2007) A broadband compact microstrip rat-race hybrid using a novel CPW inverter. *IEEE Transactions on Microwave Theory and Techniques* **55**, 161–167.
12. **Chuang M-L** (2005) Miniaturized ring coupler of arbitrary reduced size. *IEEE Microwave and Wireless Components Letters* **15**, 16–18.
13. **Eccleston KW and Ong SHM** (2003) Compact planar microstripline branch-line and rat-race couplers. *IEEE Transactions on Microwave Theory and Techniques* **51**, 2119–2125.
14. **Kuo J-T, Wu J-S and Chiou Y-C** (2007) Miniaturized rat race coupler with suppression of spurious passband. *IEEE Microwave and Wireless Components Letters* **17**, 46–48.
15. **Cheng KM and Yeung S** (2013) A novel rat-race coupler with tunable power dividing ratio, ideal port isolation and return loss performance. *IEEE Transactions on Microwave Theory and Techniques* **61**, 55–60.
16. **Cheng KM and Chick MJ** (2013) A frequency-compensated rat-race coupler with wide bandwidth and tunable power dividing ratio. *IEEE Transactions on Microwave Theory and Techniques* **61**, 2841–2847.
17. **Ang KS, Leong YC and Lee CH** (2002) A new class of multisection 180 hybrids based on cascadable hybrid-ring couplers. *IEEE Transactions on Microwave Theory and Techniques* **50**, 2147–2152.
18. **Park MJ and Byungje L** (2005) Coupled line 180 deg hybrid coupler. *Microwave and Optical Technology Letters* **45**, 173–176.
19. **Napijalo V** (2012) Coupled line 180° hybrids with Lange couplers. *IEEE Transactions on Microwave Theory and Techniques* **60**, 3674–3682.
20. **Liu H, Fang S, Wang Z and Fu S** (2014) Novel coupled line 180 hybrid with non-interspersed input output ports. *IEEE Transactions on Microwave Theory and Techniques* **62**, 2641–2649.
21. **Schiffman BM** (1958) A new class of broad-band microwave 90-degree phase shifters. *IRE Transactions on Microwave Theory and Tech* **6**, 232–237.
22. **Quirarte JLR and Starski JP** (1991) Synthesis of Schiffman phase shifters. *IEEE Transactions on Microwave Theory and Techniques* **39**, 1885–1889.
23. **Quirarte JLR and Starski JP** (1993) Novel Schiffman phase shifters. *IEEE Transactions on Microwave Theory and Techniques* **41**, 9–14.
24. **Schiffman BM** (1966) Multisection microwave phase-shift network (Correspondence). *IEEE Transactions on Microwave Theory and Techniques* **14**, 209.
25. **Schiek B and Kohler J** (1977) A method for broad-band matching of microstrip differential phase shifters. *IEEE Transactions on Microwave Theory and Techniques* **25**, 666–671.
26. **Guo Y-X, Zhang Z-Y and Ong L-C** (2006) Improved wide-band Schiffman phase shifter. *IEEE Transactions on Microwave Theory and Techniques* **54**, 1196–1200.
27. **Oraizi H and Shamsafar A** (2012) Optimum design of modified Schiffman multi-section wide band differential phase shifter with impedance matching. *Progress in Electromagnetics Research C* **29**, 1–16.
28. **Zhang W, Liu Y, Wu Y, Wang W, Su M and Gao J** (2014) A modified coupled-line Schiffman phase shifter with short reference line. *Progress in Electromagnetics Research C* **54**, 17–27.
29. **Dobrowolski JA** (1991) *Introduction to Computer Methods for Microwave Circuit Analysis and Design*, 1st Edn. Norwood, MA: Artech House Press, 22–52.
30. **Frei J, Cai XD and Muller S** (2008) Multiport *T*-parameter and *S*-parameter conversion with symmetry extension. *IEEE Transactions on Microwave Theory and Techniques* **56**, 2493–2504.
31. **Geogre GI, Zysman I and Johnson AK** (1969) Coupled transmission line networks in an inhomogeneous dielectric medium. *IEEE Transactions on Microwave Theory and Techniques* **17**, 753–759.
32. **Frickey DA** (1994) Conversions between S, Z, Y, H, ABCD, and T parameters which are valid for complex source and load impedances. *IEEE Transactions on Microwave Theory and Techniques* **42**, 205–211.
33. **Marks RB, Williams DF and Frickey DA** (1995) Comments on "Conversions between S, Z, Y, h, ABCD, and T parameters which are valid for complex source and load impedances" [with reply]. *IEEE Transactions on Microwave Theory and Techniques* **43**, 914–915.
34. **Alhalabi H, Issa H, Pistono E, Kaddour D, Podevin F, Baheti A and Ferrari P** (2018) Miniaturized branch-line coupler based on slow-wave microstrip lines. *International Journal of Microwave and Wireless Technologies* **10**, 1103–1106.

Jaber Moghaddasi received his B.Sc. degree in electrical engineering from K. N. T University of Technology, Tehran, Iran, in 2010, and his Ph.D. degree from Polytechnique Montréal in Montréal, Canada, in 2017. He has authored several peer-reviewed papers and holds three patents. He was a recipient of several awards, including the 2019 IEEE Microwave Theory and Techniques Society (MTT-S) Microwave Prize, the best paper award in the IEEE IWS-2013 in Beijing, China, and the student challenge prize in EuMW-2013 in Nuremberg, Germany. He joined *BlackBerry* Company in 2015 and worked as a co-op research engineer with Huawei Company throughout 2014. In 2017, he joined Hytera Company as an RF engineer, in Richmond, BC, Canada.

Ke Wu received the B.Sc. degree (with distinction) in radio engineering from the Nanjing Institute of Technology (now Southeast University), China, in 1982 and the D.E.A. and Ph.D. degrees in optics, optoelectronics, and microwave engineering (with distinction) from the Institut National Polytechnique de Grenoble (INPG) and University of Grenoble, France, in 1984 and 1987, respectively.

Dr. Wu is a Professor of electrical engineering, and endowed Industrial Research Chair in Future Wireless Technologies with the Polytechnique Montréal (University of Montreal), QC, Canada. He has been the Director of the Poly-Grames Research Center. He was the founding Director of the Center for Radiofrequency Electronics Research of Quebec (Regroupement stratégique of FRQNT) and Tier-I Canada Research Chair in RF and millimeter-wave engineering. Currently, he is also with the School of Information Science and Engineering, Ningbo University, on leave from his home institution. He has held guest, visiting, and honorary professorships with many universities around the world. He has authored or co-authored over 1300 referred papers and a number of books/book chapters. He has filed more than 50 patents. His current research interests involve substrate integrated circuits and systems, antenna arrays, field theory and joint field/circuit modeling, ultra-fast interconnects, wireless power transmission and harvesting, and MHz-through-THz technologies and transceivers for wireless sensors and systems as well as biomedical applications. He is also interested in the modeling and design of microwave and terahertz photonic circuits and systems.

Dr. Wu is a Fellow of the IEEE, of the Canadian Academy of Engineering (CAE), and of the Royal Society of Canada (The Canadian Academy of the Sciences and Humanities). He is a Member of Electromagnetics Academy, Sigma Xi, URSI, and IEEE-Eta Kappa Nu (IEEE-HKN). He has held key positions in and has served on various panels and international committees including the chair of Technical Program Committees, International Steering Committees, and international conferences/symposia. In particular, he was the General Chair of the 2012 IEEE Microwave Theory and Techniques (IEEE MTT-S) International Microwave Symposium (IMS). He has served on the Editorial/Review Boards of many technical journals, transactions, proceedings, and letters as well as scientific encyclopedia including Editor and Guest Editor. He was the Chair of the joint IEEE Montreal chapters of MTT-S/AP-S/LEOS and then the restructured IEEE MTT-S Montreal Chapter, Canada. He has served IEEE MTT-S and Administrative Committee (AdCom) as the Chair of the IEEE MTT-S Transnational Committee, Member and Geographic Activities (MGA)

https://doi.org/10.1017/S1759078719001533 Published online by Cambridge University Press

Committee, Technical Coordinating Committee (TCC), and 2016 IEEE MTT-S President among many other AdCom functions. Currently, he is the Chair of the IEEE MTT-S Inter-Society Committee. He was an IEEE MTT-S Distinguished Microwave Lecturer (2009–2011). Dr. Wu is the inaugural representative of North America as a Member of the European Microwave Association (EuMA) General Assembly. He was the recipient of many awards and prizes including the first IEEE MTT-S Outstanding Young Engineer Award, the 2004 Fessenden Medal of the IEEE Canada, the 2009 Thomas W. Eadie Medal of the Royal Society of Canada, the Queen Elizabeth II Diamond Jubilee Medal in 2013, the 2013 FCCP Education Foundation Award of Merit, the 2014 IEEE MTT-S Microwave Application Award, the 2014 Marie-Victorin Prize (Prix du Quebec – the highest distinction of Québec in the natural sciences and engineering), the 2015 Prix d'Excellence en Recherche et Innovation of Polytechnique Montréal, the 2015 IEEE Montreal Section Gold Medal of Achievement, and the 2019 IEEE MTT-S Microwave Prize.

https://doi.org/10.1017/S1759078719001533 Published online by Cambridge University Press